processes

MDPI

Article

Probing Element Transfer Behavior during the Submerged Arc Welding Process for CaF_2-SiO_2-Na_2O-Cr_2O_3 Agglomerated Fluxes: A Thermodynamic Approach

Jin Zhang [1,2,*] and Qiong Xu [1]

[1] School of Mechanical and Electrical Engineering, Suqian University, Suqian 223800, China
[2] School of Metallurgy, Northeastern University, Shenyang 110819, China
* Correspondence: 18142@squ.edu.cn

Abstract: Submerged arc welding joins metal by the heating of the electrode, base metal, and flux in the arc plasma, while the weld pool is protected under the granular flux and molten slag. Due to complex chemical reactions occurring between the arc plasma, weld pool, and molten slag (flux), flux essentially affects the weld metal composition, which, in turn, dictates the mechanical properties of the weldment. Therefore, fine-tuning the weld metal composition is essential to ensure a sound weld, and efforts worldwide have been focused on the control mechanism of flux on the weld metal composition. Recently, agglomerated fluxes have been widely applied due to low energy consumption during manufacture. The Cr_2O_3-bearing agglomerated flux is one of the most commonly used flux types in fields of heavy industrial applications. However, few works concern the element transfer behavior when Cr_2O_3-bearing agglomerated fluxes are used. Within this framework, typical agglomerated CaF_2-SiO_2-Na_2O-Cr_2O_3 fluxes with varying Cr_2O_3 content from 10 to 50 wt.% are designed and applied to Q345A steel. The influence of Cr_2O_3 content upon the transfer behaviors of essential elements, including O, Cr, and Mn, is quantified and interpreted from the point of thermodynamics. By incorporating a gas-slag-metal equilibrium consideration, the assumptions made in previous studies are justified. Additionally, evidence regarding the loss of Cr and Mn to the arc plasma is provided, and a possible thermodynamic approach to predict element transfer levels is proposed. It is revealed that the gas-slag-metal equilibrium consideration is able to qualitatively analyze the transfer behaviors involved in the submerged arc welding system, even under high temperatures. Based on the quantitative data, the practical implications as well as limitations of the gas-slag-metal equilibrium model are proposed.

Keywords: welding process; element transfer; welding flux; submerged arc welding

Citation: Zhang, J.; Xu, Q. Probing Element Transfer Behavior during the Submerged Arc Welding Process for CaF_2-SiO_2-Na_2O-Cr_2O_3 Agglomerated Fluxes: A Thermodynamic Approach. *Processes* **2022**, *10*, 1900. https://doi.org/10.3390/pr10101900

Academic Editor: Chin-Hyung Lee

Received: 14 June 2022
Accepted: 13 August 2022
Published: 20 September 2022

1. Introduction

Submerged arc welding (SAW) is an extremely versatile automatic arc welding method widely applied in fields of heavy industrial applications, owing to its high deposition rate and excellent reliability [1]. Since the control of WM compositions is important for producing the weldment of sound quality, an understanding of the mechanisms that alter the weld metal (WM) compositions would be a primary aid in such control [2–6].

Flux plays a complex role during the SAW process. In addition to stabilizing arc plasma, providing slag, and promoting slag detachability, flux essentially affects WM compositions due to the chemical reactions occurring between the flux (slag), weld pool, and arc plasma. Therefore, to better control WM compositions, an in-depth understanding of the element transfer behavior in SAW is necessary [7,8]. In SAW engineering, a Δ value is adopted to quantify the element transfer between flux and WM [9,10]. The Δ value may be positive or negative depending upon the element transfer direction; that is, a positive Δ value indicates an elemental gain from the flux, whereas a negative Δ value indicates an elemental loss from the WM to the slag [11–14].

Understanding the mechanisms in terms of the element transfer between flux and WM can be attained by investigating the influence of a flux chemical additive on the quantified element transfer, *viz.* the Δ value. For instance, Zhang et al. [11,12,14] designed a series of CaF_2-based fused fluxes with varying oxide addition levels and evaluated the impact of SiO_2, MnO, and TiO_2 on the element transfer between flux and WM. Dallam et al. [7] documented the influence of CaF_2, CaO, and FeO addition on the Δ values of O, Si, and Mn when manganese-silicate fluxes were used. Kanjilal et al. [15], in contrast, studied the effect of CaF_2 and NiO addition on the ΔMn value for CaF_2-CaO-SiO-Al_2O_3-based agglomerated fluxes.

However, the mechanisms responsible for the element transfer behavior in SAW due to Cr_2O_3 addition into fluxes have not been clearly described. One typical thermodynamic investigation was conducted by Mitra et al. [16]; nonetheless, within the above work, the levels of Cr_2O_3 in fluxes were confined in a narrow range from 10 to 18 wt.%.

Cr_2O_3-bearing fluxes are widely applied when heat-resistant steel is submerged-arc-welded. The C_2O_3 in the flux exerts a significant impact on the contents of O and Cr of the submerged-arc-welded metal, which, in turn, dictates the mechanical properties of the weld. Therefore, a deep understanding of the transfer behavior in SAW when Cr_2O_3-bearing fluxes are applied is essential [17–20].

The objective of this study is to investigate the influence of Cr_2O_3 on the element transfer behavior from the point of thermodynamics over a wide compositional range of Cr_2O_3 in fluxes. By using agglomerated fluxes, the role of Cr_2O_3 in the determination of WM final compositions is qualified. By incorporating a gas-slag-metal equilibrium consideration, the quantified Δ values are interpreted and several assumptions regarding the transfer of elements are justified thermodynamically. Additionally, evidence regarding the loss of Cr and Mn to the arc plasma is provided by using measured data, and a possible thermodynamic approach to predict the Δ values for Cr_2O_3-bearing fluxes is suggested.

2. Materials and Methods

2.1. Flux Preparation

For each flux recipe, 1 kg of reagent-grade powders were weighted according to the formulas given in Table 1. In addition to Cr_2O_3, CaF_2 (the non-oxide with no O potential) was added as a diluent to lower the melting temperature of the flux [21]. The powders were mixed in a V blender at 0.5 Hz for an hour. Then, the powders were bonded by a 150 g sodium-silicate solution; as such, SiO_2 and Na_2O are incorporated since they help improve the slag detachability and arc stability [10,14]. Subsequently, the bonded mixtures were pelletized and dried in a muffle furnace at 973 K for 3 hours. At last, the mixtures were broken up and screened to a 14 to 100 mesh [9]. In this study, "flux" means the starting material before SAW, while "slag" implies the molten or solidified flux during or after SAW [8,22].

Table 1. Formulas of initial fluxes (wt.%).

Flux	Cr_2O_3	CaF_2
F-1	10	90
F-2	20	80
F-3	30	70
F-4	40	60
F-5	50	50

2.2. Welding Experiment

A typical low alloy grade steel, Q345A, was selected as the base metal (BM). Bead-on-plate double-electrode single-pass SAW (Lincoln Electric Power Wave AC/DC 1000 SD, Lincoln Electric, Cleveland, OH, USA) was performed at a heat input of 60 kJ/cm (DC-850 A/32 V for electrode forward, AC-625 A/36 V for electrode backward, 500 mm/min).

2.3. Chemical Composition Analysis

X-ray fluorescence (XRF, model S4 Explorer, Bruker, Germany) was used to determine the compositions of fluxes and slags. The content of F was determined by a titration method. The analytical compositions of fluxes and slags are given in Tables 2 and 3, where the basicity index (*BI*) of each flux is determined by Equation (1) [23].

Table 2. Measured compositions of fluxes (wt.%).

Flux	Cr_2O_3	SiO_2	Na_2O	CaF_2	*BI*
F-1	12.58	7.99	0.52	78.91	5.56
F-2	22.89	7.56	0.48	69.07	3.66
F-3	32.88	7.63	0.55	58.94	2.47
F-4	41.99	7.88	0.61	49.52	1.74
F-5	53.19	7.66	0.49	38.66	1.14

Table 3. Measured compositions of slags (wt.%).

Flux	Cr_2O_3	SiO_2	Na_2O	FeO	MnO	Al_2O_3	TiO_2	CaF_2
F-1	5.63	8.1	0.25	4.65	3.54	0.18	0.11	76.75
F-2	11.25	8.52	0.21	7.26	4.25	0.17	0.10	67.41
F-3	18.11	8.22	0.28	10.37	5.50	0.20	0.10	56.46
F-4	24.72	8.58	0.21	12.41	5.30	0.21	0.13	47.41
F-5	32.45	10.11	0.14	13.91	6.66	0.2	0.11	35.63

Only components > 0.1 wt.% were taken into account.

$$BI = \frac{CaO + CaF_2 + MgO + Na_2O + K_2O + 0.5 \times (MnO + FeO)}{SiO_2 + 1/2(Al_2O_3 + Cr_2O_3 + TiO_2 + ZrO_2)} \quad (1)$$

Inductively coupled plasma optical emission spectrometry (ICP-OES, Perkin Elmer) was used to determine the compositions of metallic elements, while the LECO analyzer was used to determine the contents of O. The compositions of the electrode and BM are given in Table 4.

Table 4. Measured chemical compositions of the BM and electrode (wt.%).

	C	Si	Mn	Ti	Cr	O
Q345A	0.112	0.142	1.540	0.015	0.018	0.003
Electrode	0.127	0.049	1.650	0.015	0.015	0.003

The Δ values for O, Cr, and Mn are quantified from Equation (2).

$$\Delta = M_{WM} - M_N \quad (2)$$

In Equation (2), M_{WM} is the measured WM composition, while M_N is the nominal composition (the composition considering only the dilution effect of the BM and electrode) [9,12,14]. The M_N value is determined from Equation (3), where M_{BM} represents the measured composition of the BM, M_{el} represents the measured composition of electrode, and d represents the dilution value of the BM.

$$M_N = M_{BM} \times d + M_{el} \times (1 - d) \quad (3)$$

To determine the value of d, the weldments were cross-sectioned, polished, and etched by a 4 wt.% nital solution. Then, the value of d was calculated from Equation (4).

$$d = \frac{\text{Area of fused base metal}}{\text{Area of weld metal}} \quad (4)$$

The data of nominal compositions, measured WM compositions, and Δ values for O, Cr, and Mn are summarized in Table 5.

Table 5. Nominal compositions, measured WM compositions, and quantified Δ values (wt.%).

Weld Metal	WM-1	WM-2	WM-3	WM-4	WM-5
Flux	**F-1**	**F-2**	**F-3**	**F-4**	**F-5**
$(O)_A$	0.049	0.074	0.118	0.147	0.162
$(O)_N$	0.003	0.003	0.003	0.003	0.003
ΔO	0.046	0.071	0.115	0.144	0.159
$(Cr)_A$	1.050	1.620	1.800	2.080	2.620
$(Cr)_N$	0.016	0.017	0.017	0.017	0.016
ΔCr	1.034	1.603	1.783	2.063	2.604
$(Mn)_A$	0.710	0.510	0.310	0.260	0.190
$(Mn)_N$	1.601	1.593	1.586	1.591	1.616
ΔMn	−0.891	−1.083	−1.276	−1.331	−1.426

2.4. Thermodynamic Calculation

Due to the limited understanding of the SAW process, researchers often used the "effective equilibrium temperature" to perform a thermodynamic equilibrium calculation [22,24,25]. The effective equilibrium temperature does not imply the measured equilibrium temperature of SAW but indicates the temperature at which the experimental mass action index equals the equilibrium constant. Within this framework, the effective equilibrium temperature was set to 1973 and 2273 K, which was concluded by Mitra et al. [16] when Cr_2O_3-bearing fluxes were applied.

Recently, interactions at the gas-slag-metal interface in SAW have been documented [1,26]. Major phases and reaction interfaces associated with gas phases are given in Figure 1a; the blue point in Figure 1c indicates the plasm(gas)-slag-gas interface, while the green point in Figure 1b indicates the bubble(gas)-slag-gas interface [26]. As was concluded in our previous study, the nucleation and release of bubbles are closely related to complex factors, although the mechanisms are not fully understood; nonetheless, the existence of arc plasma guarantees the existence of a bubble(gas)-slag-gas interface [26].

There are two issues complicating the investigation over the development of the compositional prediction model for SAW [27]:

1. It is impossible to capture the gases in the arc plasma and to sample the molten slag for analytical purposes since the arc plasma, molten slag, and weld pool are shielded under the flux during the SAW process.
2. The effective equilibrium temperature of the SAW chemical system is as high as 2000 °C, under which the thermodynamic information remains scarce.

Hopefully, a number of thermodynamic databases for gases, oxides, and alloy systems have been developed by the Calphad technique in recent decades [28,29]. Additionally, with the help of the applicable thermodynamic models (such as the cell model and the modified regular solution model), the thermodynamic data could be extended to a SAW temperature as high as 2273 K [30].

In this regard, gas-slag-metal equilibrium calculations were performed at temperatures of 1973 and 2273 K to aid in the discussion on the quantified element transfer data. This approach was used in our previous study to illustrate the transfer of Ti and O from TiO_2-bearing basic-fluoride fluxes to WMs subject to varying TiO_2 levels [31]. The details of the thermodynamic calculation are given in Appendix A.

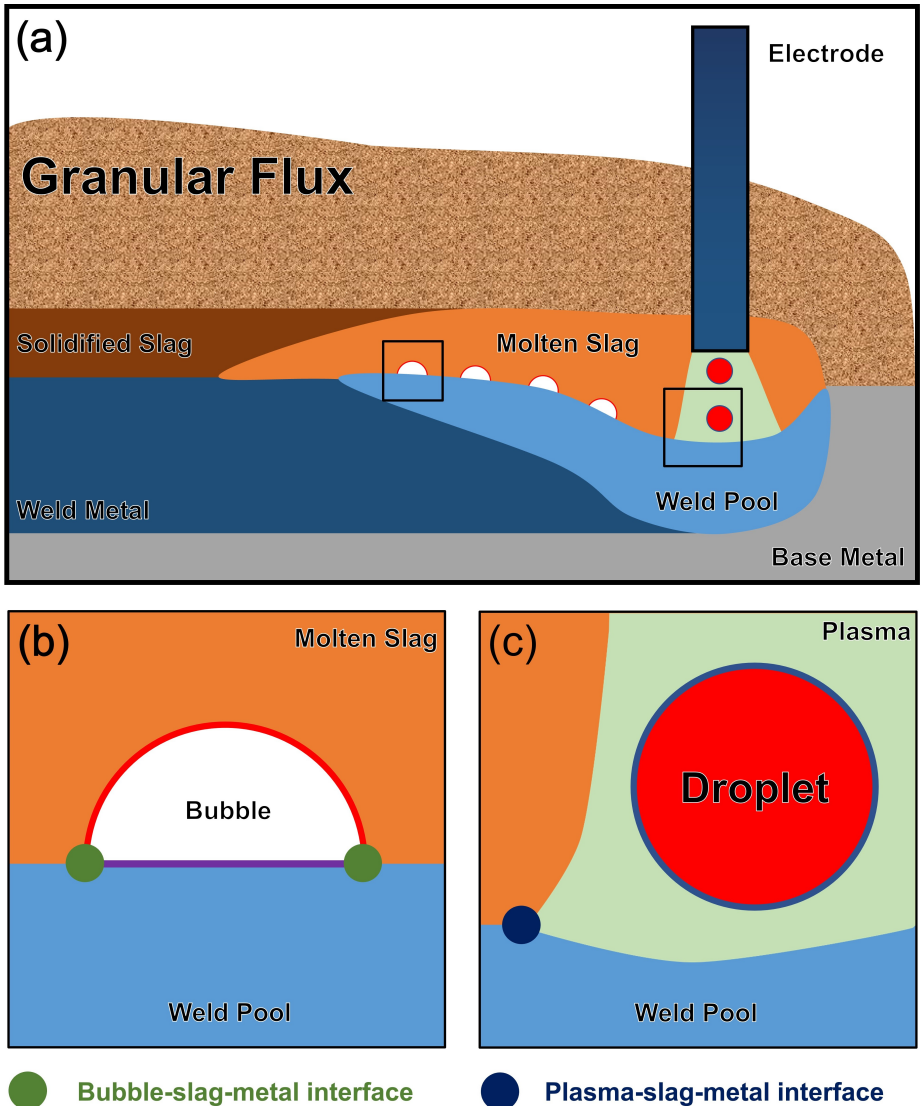

Figure 1. Major phases and reaction interfaces associated with gas phases in SAW: (**a**) Schematic diagram of SAW, (**b**) Plasma-associated reaction interfaces, (**c**) Bubble-associated reaction interfaces.

3. Results and Discussion

3.1. Transfer of O

O is one of the most essential elements for submerged-arc-welded metal that must be carefully controlled [32]. It is accepted that excessive O in the WM tends to cause several problems, such as promoting porosity, reducing toughness, and decreasing hardenability [10,25]. However, a WM with too low O levels shows poor impact toughness since there are insufficient inclusions to promote the formation of acicular ferrite (AF) [33,34].

In comparison to other arc welding methods, one salient feature of the SAW process is the significant O uptake from the flux [10,35]. Chai et al. [21] assumed that under the presence of an arc plasma of high temperature, oxide in the flux tends to decompose into suboxides, releases O_2 gas in the arc cavity, and transfers O to the weld pool. Based on an observation from Tables A2 and A3, Cr_2O_3 and CrO are the primary Cr oxides in the slag. Therefore, based on the assumption made by Chai et al. [21], it is speculated that Cr_2O_3 tends to decompose into CrO and O_2 gas via Reaction (5) at the flux(slag)-plasma interface.

$$2(Cr_2O_3) = 4(CrO) + O_2(g) \quad (5)$$

An empirical concept of the flux basicity index (*BI*) has been adopted to identify the flux O potential (the driving force for O transfer from the flux to the WM); generally,

a higher *BI* value means a lower flux O potential, and, thus, a lower O content of the submerged-arc-welded metal [9,10]. Based on the experimental data, a general relationship between the weld metal O content and the flux *BI* is summarized in Figure A1, based on which the O content can be predicted from the flux *BI* [23].

Another prediction approach was developed by Zhang et al. [31], in which the O level was predicted from the gas-slag-metal equilibrium calculations; this approach was based on the assumed local attained gas-slag-metal thermodynamic equilibrium involved in the SAW process. The predicted data from the *BI* model and the gas-slag-metal equilibrium model for O contents are given in Figure 2.

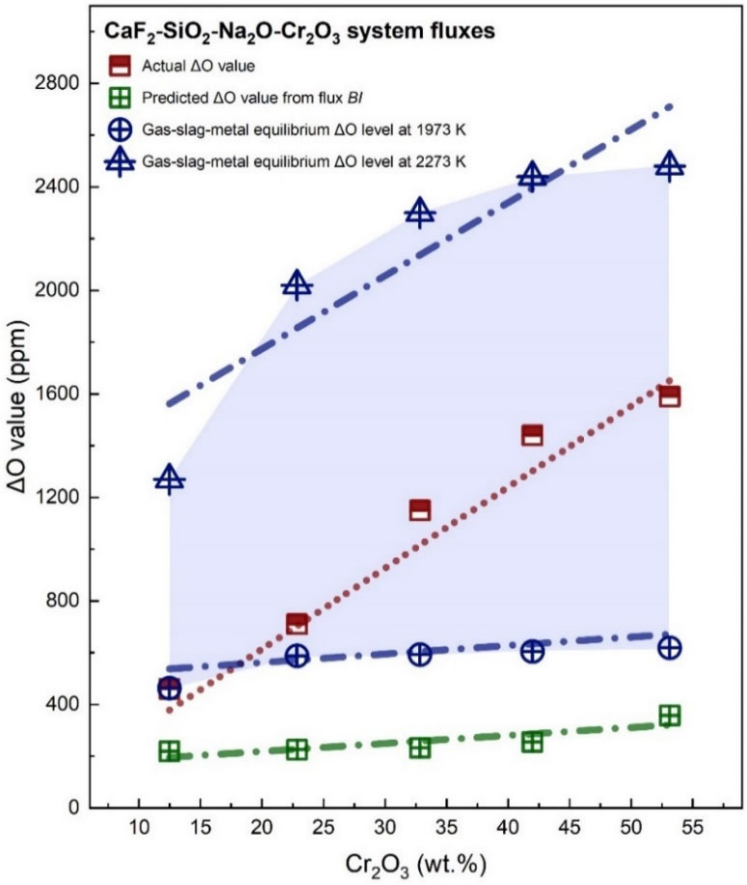

Figure 2. Actual and predicted ΔO levels as a function of the Cr_2O_3 addition level in the flux.

Based on an observation from Figure 2, both the flux *BI* and gas-slag-metal equilibrium models are capable of predicting the upward changing trend of ΔO values with a higher addition level of Cr_2O_3 in the flux (see the green and blue dot-dash lines in Figure 2). Specially, as shown by the blue-shaded area in Figure 2, the measured ΔO values lay in the ranges calculated by the gas-slag-metal equilibrium calculations at 1973 and 2273 K. Therefore, the consideration of the gas-slag-metal equilibrium is able to place limits on the transfer of O between flux and WM.

Additionally, as was assumed by Lau et al. [36] and Mitra et al. [37], the O uptake from the flux is governed by the level of O_2 gas pressure in the arc plasma. To verify this assumption, the gas-slag-metal equilibrium O_2 gas pressure was calculated and is provided in Tables A3 and A4, from which it is seen that the gas-slag-metal equilibrium O_2 gas pressure generally increases with a higher level of Cr_2O_3 addition in the flux.

Another parameter to identify the flux O potential is the FeO uptake in the slag [16,37,38]. Considering Reaction (6) occurring at the slag-metal interface, Zhang et al. [11,12,14] assumed that the FeO level in the slag is proportional to the WM O content since a higher flux O potential tends to drive Reaction (6) to the right side, resulting in a higher level of

FeO uptake in the slag. This assumption is confirmed by the increasing FeO content in the slag with Cr_2O_3 addition (corresponding to a higher flux O potential), as shown by the red dash line in Figure 3.

$$[Fe] + [O] = (FeO) \quad (6)$$

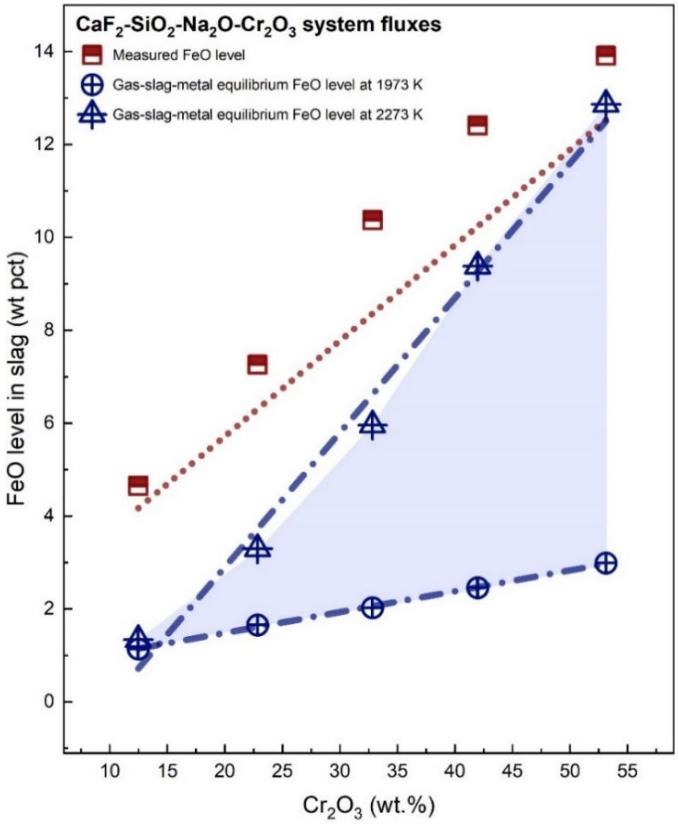

Figure 3. FeO level in the slag as a function of the Cr_2O_3 addition level in the flux.

However, it is noted that the measured FeO level was higher than the gas-slag-metal equilibrium ones, as shown in Figure 3. This phenomenon can be explained by the assumption proposed by Mitra et al. [38], that is, Reaction (6) only proceeds forward, and the equilibrium of Reaction (6) is not attained. The measured FeO level in this work may provide the evidence proposed by Mitra et al. [38] regarding the transfer of Fe in previous studies.

3.2. Transfer of Cr

Figure 4 illustrates the levels of the actual and predicted ΔCr values as a function of the Cr_2O_3 addition level in the flux. As shown by the blue-shaded area in Figure 4, the incumbent approach is capable of placing a limit on the values of ΔCr, except at 12.48 wt.% Cr_2O_3. Mitra et al. [16] assumed that the transfer of Cr between Cr_2O_3-bearing fluxes and submerged arc welded metals governed by Reaction (7) at the slag-metal interface; to check whether such assumption is feasible for this study, the activities of Cr oxides calculated from the gas-slag-metal equilibrium model are plotted in Figure 4 to aid in the analysis [31,39].

$$(Cr_2O_3) = 2[Cr] + 3[O] \quad (7)$$

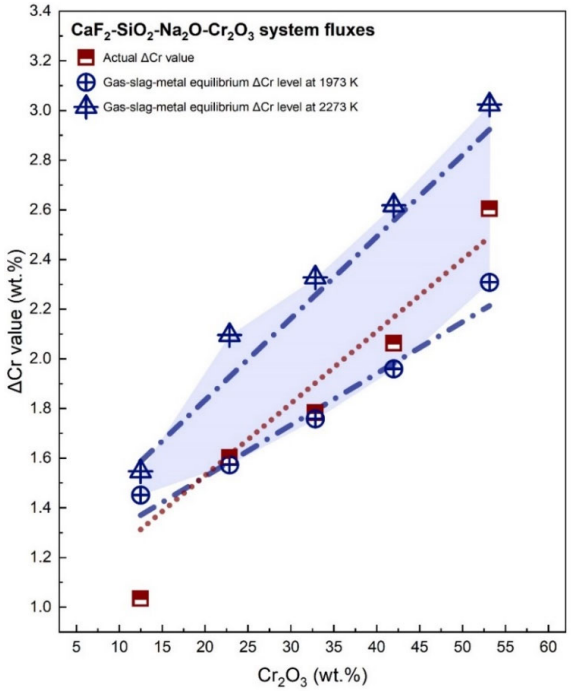

Figure 4. Actual and predicted ΔCr levels as a function of the Cr_2O_3 addition level in the flux.

It seems that the sole consideration of Reaction (7) is insufficient to explain the transfer behavior of Cr for this case study. As was demonstrated in our previous study, the transfer between the suboxide and the weld pool, such as Reaction (8) at the slag-metal interface, should be considered in terms of transfer for an alloy element [31].

$$(CrO) = [Cr] + [O] \quad (8)$$

As shown in Figure 5b, the activities of CrO in the molten slag were much higher than those of Cr_2O_3. Considering the conclusion that the level of element transfer is essentially controlled by the oxide activity in the slag, it is speculated that Reaction (8) should be considered regarding the transfer of Cr, which is rather remarkable and different from the previous assumption raised by Mitra et al. [14,16,31]. As such, it is speculated that the improvement of both Cr_2O_3 and CrO activity drives Reaction (8) to the right side, leading to a higher level of ΔCr with Cr_2O_3 addition to the flux, even at a higher flux O potential.

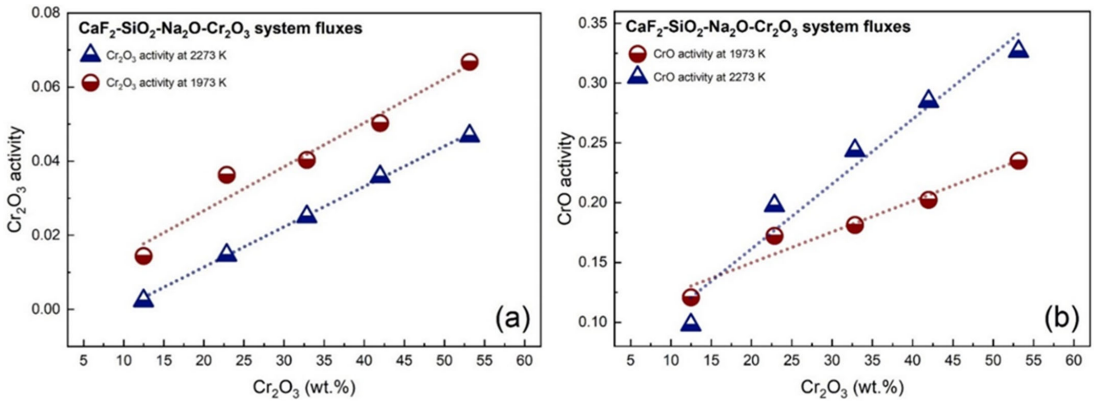

Figure 5. Gas-slag-metal equilibrium activities of Cr oxides: (**a**) Activity of Cr_2O_3, (**b**) Activity of CrO.

Additionally, it is well known that the loss of Cr tends to occur in SAW. Such loss is confirmed by the mass balance calculation given in Appendix A. Glasser et al. [40] assumed that Cr is lost from the silicate mixtures in the form of trivalent Cr. Based on an observation

from Tables A3 and A4, CrF_3 is the primary Cr-contained gas generated in the SAW process. Therefore, the gas-slag-metal equilibrium model may justify the assumption raised by Glasser et al. [40].

3.3. Transfer of Mn

The levels of ΔMn calculated from the gas-slag-metal equilibrium model are plotted in Figure 6. It is seen that the gas-slag-metal equilibrium model is able to predict the transfer direction of Mn between the flux and the submerged-arc-welded metal, *viz*. the negative ΔMn values (see the blue circles and triangles in Figure 6). Especially, the ΔMn values are constrained by using the gas-slag-metal equilibrium model, as shown by the red squares and the blue-shaded area in Figure 6. Similar to the case of Cr transfer, Mn tends to be lost from the SAW system via gas formation, which is confirmed by the mass balance calculation in Appendix A.

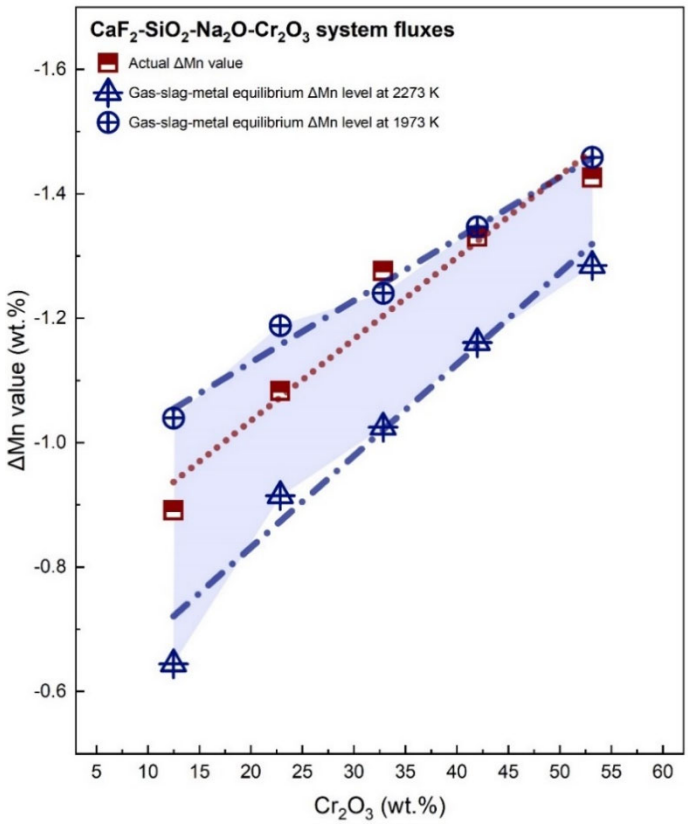

Figure 6. Actual and predicted ΔMn levels as a function of the Cr_2O_3 addition level in the flux.

Mn is an essential element for a WM. Mn is an AF-promoting agent, and its level, ranging from 0.6 to 1.8 wt.%, could increase the AF fraction and depress the formation of polygonal and side plate ferrites [26]. Therefore, an electrode and/or a BM with higher Mn levels is recommended to match the Cr_2O_3-bearing flux, thereby compensating the possible Mn loss incurred by oxidation reactions.

4. Conclusions

Within this framework, the transfer behaviors of O, Cr, and Mn involved in SAW were quantified and evaluated from a thermodynamic perspective when CaF_2-SiO_2-Na_2O-Cr_2O_3 system fluxes were used. The following conclusions can be drawn:

1. By performing a gas-slag-metal thermodynamic equilibrium calculation, the transfer direction of O, Cr, and Mn can be detected and the level of element transfer (ΔO, ΔCr,

and ΔMn) can be constrained, which may pave a viable way for the prediction of element transfer behaviors when Cr_2O_3-bearing fluxes are applied.
2. The measured slag compositions, coupled with thermodynamic data, demonstrated that the thermodynamic equilibrium for Fe transfer is not achieved.
3. The loss of Mn from the weld pool is enhanced due to a higher level of Cr_2O_3 addition to the flux. The evidence regarding the loss of Cr and Mn from the SAW system to the gas phase was provided; such loss is predictable by using a gas-slag-metal equilibrium model.
4. An electrode and/or a BM with higher Mn levels is recommended to match the Cr_2O_3-bearing flux, thereby compensating the possible Mn loss incurred by oxidation reactions.
5. The content of Cr_2O_3 in the flux should be controlled under 30 wt.% since a WM with an O level higher than 1000 ppm may incur unexpected issues, such as enhanced porosity, reduced toughness, and depreciated hardenability.
6. With a higher level of Cr_2O_3 addition to the flux, the Cr contents in the electrode and the BM should be restricted to avoid redundant Cr uptake from the flux.

Nonetheless, the measurement of thermodynamic data at ultra-high temperature is still a technical problem. Therefore, the author suggests that the limitations of this work are that:

1. Since the high-temperature thermodynamic data are extended from the model, there must be an error with the real and predicted data.
2. FactSage only considers the assumed thermodynamic equilibrium involved in SAW. However, kinetic factors should also be considered to improve the overall accuracy.
3. More work on SAW experiments is required to determine the optimal calculation temperature.

Author Contributions: Conceptualization, J.Z.; methodology, software, J.Z. and Q.X. All authors have read and agreed to the published version of the manuscript.

Funding: This work was financially supported by the National Natural Science Foundation of China (No. 52171031), the Fundamental Research Funds for the Central Universities (No. N2225011), the Initial Fund of Suqian University (No. 2022XRC040), the Suqian Sci&Tech Program (No. K202113), and the Natural Science Research Program of Jiangsu Higher Education Institutions (No. 21KJB430015). We thank Dan Zhang (Department of Science and Technology, Suqian University, Suqian 223800, China) and Zhongqiu Liu (School of Metallurgy, Northeastern University, Shenyang 110819, China) for the supports on experiment and equipment.

Conflicts of Interest: On behalf of all authors, the corresponding author states that there is no conflict of interest.

Appendix A. Gas-Slag-Metal Thermodynamic Equilibrium Calculation

The mass ratio of slag to the WM was estimated from Equation (A1); in Equation (A1), the mass ratio of slag to the consumed electrode ($R_{slag/el}$) was measured following the procedure stated elsewhere [41].

$$R_{slag/WM} = R_{slag/el} \times (1 - d_{BM}) \quad \text{(A1)}$$

The values of d_{BM} and $R_{slag/WM}$ are given in Table A1.

Then, the Equilib module of FactSage was used to perform gas-slag-metal equilibrium calculations by following the settings in our previous study [31,39,41–43]:

1. FToxid, Fstel, and FactPS databases were selected. The solution phases of ASlag-liq all oxides, S (FToxid-SLAGA), and LIQUID (FStel-Liqu) were selected to model the molten slag and steel phases.
2. The equilibrium temperature in SAW was set to 1973 and 2273 K.
3. A nominal composition, which refers to the contents considering only the dilution effects of the BM and electrode [7,8], was used as input metal chemistries, as shown in Table A2 (the subscript N indicates nominal compositions).

4. The mass ratio of the flux to the electrode was set according to the measured data in Table A1. The measured composition of the flux in Table 2 was set as input flux chemistries. The predicted Δ_p value is calculated from Equation (A2), where M_P indicates the predicted composition and M_N indicates the nominal composition.

$$\Delta_p = M_p - M_N \quad \text{(A2)}$$

Parts of outputs for discussion purposes are given in Table A3 (performed under 1973 K) and Table A4 (performed under 2273 K).

Table A1. The d_{BM} value and estimated mass ratio of slag to WM (wt.%).

Weld Metal	**WM-1**	**WM-2**	**WM-3**	**WM-4**	**WM-5**
Flux	**F-1**	**F-2**	**F-3**	**F-4**	**F-5**
d_{BM}	0.454	0.524	0.579	0.536	0.414
$R_{slag/WM}$	0.233	0.211	0.182	0.192	0.221

Table A2. The summary of metal nominal compositions (wt.%).

	WM-1	**WM-2**	**WM-3**	**WM-4**	**WM-5**
$(C)_N$	0.120	0.119	0.118	0.119	0.121
$(Si)_N$	0.091	0.098	0.103	0.099	0.088
$(Mn)_N$	1.600	1.592	1.586	1.591	1.604
$(Ti)_N$	0.015	0.015	0.015	0.015	0.015
$(Cr)_N$	0.016	0.017	0.017	0.017	0.016
$(O)_N$	0.003	0.003	0.003	0.003	0.003

Table A3. Parts of the gas-slag-metal equilibrium calculation outputs under 1973 K for 100 g WM.

Weld Metal		**WM-1**	**WM-2**	**WM-3**	**WM-4**	**WM-5**
Flux		**F-1**	**F-2**	**F-3**	**F-4**	**F-5**
CrF_3	Vol.%	3.824	4.800	5.354	6.322	7.620
MnF_2		1.366	1.042	0.930	0.684	0.415
O_2	10^{-10} atm.	4.691	7.198	7.230	7.248	7.562
CrO	Weight (g)	0.215	0.302	0.276	0.322	0.411
Cr_2O_3		0.018	0.032	0.027	0.025	0.026
FeO		0.266	0.320	0.298	0.329	0.373

Table A4. Parts of the gas-slag-metal equilibrium calculation outputs under 2273 K for WM of 100 g.

Weld Metal		**WM-1**	**WM-2**	**WM-3**	**WM-4**	**WM-5**
Flux		**F-1**	**F-2**	**F-3**	**F-4**	**F-5**
CrF_3	Vol.%	8.269	11.990	11.883	11.710	10.479
MnF_2		5.770	4.291	3.309	2.342	1.489
O_2	10^{-8} atm.	3.520	8.240	10.420	11.400	12.280
CrO	Weight (g)	0.155	0.548	0.996	1.947	1.010
Cr_2O_3		0.008	0.065	0.165	0.374	0.233
FeO		0.301	0.679	1.070	1.837	0.967

Appendix B.

The Cr loss (Cr_{loss}) from slag and metal to the gas phase is calculated from Equation (A3) [16].

$$Cr_{loss} \simeq \frac{M(Cr_i - Cr_f)}{100} + \frac{S[(Cr_2O_3)_i - (Cr_2O_3)_f]}{100} \times \frac{2(A.W.)_{Cr}}{(M.W.)_{Cr_2O_3}} \quad (A3)$$

where

M: weight of WM;
S: weight of slag;
Cr_i: initial Cr content in WM;
Cr_f: final Cr content in WM;
$(Cr_2O_3)_i$: Cr_2O_3 content in flux;
$(Cr_2O_3)_f$: Cr_2O_3 content in slag;
$(A.W.)_{Cr}$: atomic weight of Cr;
$(M.W.)_{Cr_2O_3}$: atomic weight of Cr_2O_3.

Herein, we set M to 100 g and calculated the Cr loss from the SAW system. Similarly, the Mn loss from slag and metal is calculated from Equation (A4).

$$Mn_{loss} \simeq \frac{M(Mn_i - Mn_f)}{100} + \frac{S[(MnO)_i - (MnO)_f]}{100} \times \frac{(A.W.)_{Mn}}{(M.W.)_{MnO}} \quad (A4)$$

where

M: weight of WM;
S: weight of slag;
Mn_i: initial Mn content in WM;
Mn_f: final Mn content in WM;
$(MnO)_i$: MnO content in flux;
$(MnO)_f$: MnO content in slag;
$(A.W.)_{Mn}$: atomic weight of Mn;
$(M.W.)_{MnO}$: atomic weight of MnO.The estimated Cr_{loss} and Mn_{loss} are given in Table A5.

Table A5. The estimated Cr_{loss} and Mn_{loss} values for 100 g WM (g).

Weld Metal	WM-1	WM-2	WM-3	WM-4	WM-5
Flux	**F-1**	**F-2**	**F-3**	**F-4**	**F-5**
Cr_{loss}	0.074	0.077	0.056	0.205	0.531
Mn_{loss}	0.252	0.389	0.501	0.543	0.286

Appendix C. Prediction of O Content from Flux *BI*

O contents were predicted from Figure A1 by using the flux *BI* values in Table 2.

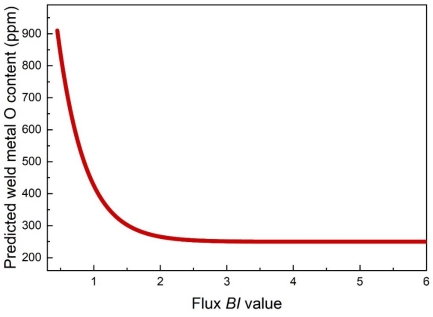

Figure A1. Predicted O content of WM as a function of the flux *BI* value [23,44].

References

1. Sengupta, V.; Havrylov, D.; Mendez, P. Physical Phenomena in the Weld Zone of Submerged Arc Welding-A Review. *Weld. J.* **2019**, *98*, 283–313. [CrossRef]
2. Coetsee, T. The Role of Metallic Iron in Low Temperature Carbothermic Reduction of MnO: Phase Chemistry and Thermodynamic Analysis. *Minerals* **2021**, *11*, 1205. [CrossRef]
3. Coetsee, T.; De Bruin, F. In Situ Modification of CaF_2-SiO_2-Al_2O_3-MgO Flux Applied in the Aluminium-Assisted Transfer of Titanium in the Submerged Arc Welding of Carbon Steel: Process Mineralogy and Thermochemical Analysis. *Minerals* **2022**, *12*, 604. [CrossRef]
4. Coetsee, T.; De Bruin, F. Aluminium Assisted Nickel Alloying in Submerged Arc Welding of Carbon Steel: Application of Unconstrained Metal Powders. *Appl. Sci.* **2022**, *12*, 5392. [CrossRef]
5. Coetsee, T.; De Bruin, F. Aluminium-Assisted Alloying of Carbon Steel in Submerged Arc Welding: Application of Al-Cr-Ti-Cu Unconstrained Metal Powders. *Processes* **2022**, *10*, 452. [CrossRef]
6. Coetsee, T.; De Bruin, F. Chemical Interaction of Cr-Al-Cu Metal Powders in Aluminum-Assisted Transfer of Chromium in Submerged Arc Welding of Carbon Steel. *Processes* **2022**, *10*, 296. [CrossRef]
7. Burck, P.; Indacochea, J.; Olson, D. Effects of Welding Flux Additions on 4340 Steel Weld Metal Composition. *Weld. J.* **1990**, *3*, 115–122.
8. Indacochea, J.E.; Blander, M.; Christensen, N.; Olson, D.L. Chemical Reactions During Submerged Arc Welding with FeO-MnO-SiO_2 Fluxes. *Metall. Trans. B* **1985**, *16*, 237–245. [CrossRef]
9. Natalie, C.A.; Olson, D.L.; Blander, M. Physical and Chemical Behavior of Welding Fluxes. *Annu. Rev. Mater. Sci.* **1986**, *16*, 389–413. [CrossRef]
10. Olson, D.; Liu, S.; Frost, R.; Edwards, G.; Fleming, D. Nature and Behavior of Fluxes Used for Welding. *ASM Int. ASM Handb.* **1993**, *6*, 55–63. [CrossRef]
11. Zhang, J.; Coetsee, T.; Dong, H.; Wang, C. Element Transfer Behaviors of Fused CaF_2-TiO_2 Fluxes in EH36 Shipbuilding Steel during High Heat Input Submerged Arc Welding. *Metall. Mater. Trans. B* **2020**, *51*, 1953–1957. [CrossRef]
12. Zhang, J.; Coetsee, T.; Dong, H.; Wang, C. Element Transfer Behaviors of Fused CaF_2-SiO_2-MnO Fluxes under High Heat Input Submerged Arc Welding. *Metall. Mater. Trans. B* **2020**, *51*, 885–890. [CrossRef]
13. Zhang, J.; Coetsee, T.; Dong, H.; Wang, C. Fine-Tuned Element Transfer Strategies for Ternary CaF_2-SiO_2-CaO Fluxes in Submerged Arc Welding: An Environmentally Friendly Approach. *Metall. Mater. Trans. B* **2020**, *51*, 1350–1354. [CrossRef]
14. Zhang, J.; Coetsee, T.; Wang, C. Element Transfer Behaviors of Fused CaF_2-SiO_2 Fluxes Subject to High Heat Input Submerged Arc Welding. *Metall. Mater. Trans. B* **2020**, *51*, 16–21. [CrossRef]
15. Kanjilal, P.; Pal, T.; Majumdar, S. Prediction of Element Transfer in Submerged Arc Welding. *Weld. J.* **2007**, *10*, 40.
16. Mitra, U.; Eagar, T. Slag Metal Reactions During Submerged Arc Welding of Alloy Steels. *Metall. Trans. A* **1984**, *15*, 217–227. [CrossRef]
17. Li, Y.; Tang, H.; Lai, R. Microstructure and Mechanical Performance of Resistance Spot Welded Martensitic Advanced High Strength Steel. *Processes* **2021**, *9*, 1021. [CrossRef]
18. Pfennig, A.; Wolf, M.; Kranzmann, A. Corrosion and Corrosion Fatigue of Steels in Downhole CCS Environment—A Summary. *Processes* **2021**, *9*, 594. [CrossRef]
19. Liu, J.; Li, Y. Influence of 12Cr1MoV Material on Tissue Properties at High Temperature and Long Operating Time. *Processes* **2022**, *10*, 192. [CrossRef]
20. Czapla, A.; Ganesapillai, M.; Drewnowski, J. Composite as a Material of the Future in the Era of Green Deal Implementation Strategies. *Processes* **2021**, *9*, 2238. [CrossRef]
21. Chai, C.; Eagar, T. Slag Metal Reactions in Binary CaF_2-Metal Oxide Welding Fluxes. *Weld. J.* **1982**, *61*, 229–232.
22. Chai, C.; Eagar, T. Slag-Metal Equilibrium during Submerged Arc Welding. *Metall. Trans. B* **1981**, *12*, 539–547. [CrossRef]
23. Tuliani, S.; Boniszewski, T.; Eaton, N. Notch Toughness of Commercial Submerged Arc Weld metal. *Weld. Met. Fabr.* **1969**, *37*, 327–339.
24. Chai, C.; Eagar, T. Prediction of Weld-metal Composition during Flux-shielded Welding. *J. Mater. Energy Syst.* **1983**, *5*, 160–164. [CrossRef]
25. Chai, C.-S. Slag-Metal Reactions during Flux Shielded Arc Welding. Ph.D. Thesis, Massachusetts Institute of Technology, Cambridge, MA, USA, 1980.
26. Zhang, J.; Coetsee, T.; Dong, H.; Wang, C. Elucidating the Roles of SiO_2 and MnO upon Decarburization during Submerged Arc Welding: A Thermodynamic Study into EH36 Shipbuilding Steel. *Metall. Mater. Trans. B* **2020**, *51*, 1805–1812. [CrossRef]
27. Cong, W.; Zhang, J. Fine-tuning Weld Metal Compositions *via* Flux Optimization in Submerged Arc Welding: An Overview. *Acta Metall. Sin.* **2022**, *57*, 1126–1140. [CrossRef]
28. Bale, C.W.; Chartrand, P.; Degterov, S.; Eriksson, G.; Hack, K.; Mahfoud, R.B.; Melançon, J.; Pelton, A.; Petersen, S. FactSage Thermochemical Software and Databases. *Calphad* **2002**, *26*, 189–228. [CrossRef]
29. Bale, C.W.; Bélisle, E.; Chartrand, P.; Decterov, S.; Eriksson, G.; Gheribi, A.; Hack, K.; Jung, I.-H.; Kang, Y.-B.; Melançon, J. Reprint of: FactSage Thermochemical Software and Databases, 2010–2016. *Calphad* **2016**, *55*, 1–19. [CrossRef]
30. Jung, I.-H. Overview of the Applications of Thermodynamic Databases to Steelmaking Processes. *Calphad* **2010**, *34*, 332–362. [CrossRef]

31. Zhang, J.; Coetsee, T.; Basu, S.; Wang, C. Impact of Gas Formation on the Transfer of Ti and O From TiO_2-bearing Basic-fluoride Fluxes to Submerged Arc Welded Metals: A Thermodynamic Approach. *Calphad* **2020**, *71*, 102195. [CrossRef]
32. Chaveriat, P.; Kim, G.; Shah, S.; Indacochea, J. Low Carbon Steel Weld Metal Microstructures: The Role of Oxygen and Manganese. *J. Mater. Eng.* **1987**, *9*, 253–267. [CrossRef]
33. Dallam, C.; Liu, S.; Olson, D. Flux Composition Dependence of Microstructure and Toughness of Submerged Arc HSLA Weldments. *Weld. J.* **1985**, *64*, 140–151.
34. Ito, J.; Nakanishi, M. Study on Charpy Impact Properties of Weld Metal with Submerged-arc Welding. *Weld. J.* **1976**, *15*, 42–62.
35. Kou, S. *Welding Metallurgy*, 3rd ed.; JohnWiley & Sons, Inc.: Hoboken, NJ, USA, 2003; pp. 22–122.
36. Lau, T.; Weatherly, G.; McLean, A. The Sources of Oxygen and Nitrogen Contamination in Submerged Arc Welding Using CaO-Al_2O_3 Based Fluxes. *Weld. J.* **1985**, *64*, 343–347.
37. Mitra, U.; Eagar, T. Slag-metal Reactions during Welding: Part II. Theory. *Metall. Trans. B* **1991**, *22*, 73–81. [CrossRef]
38. Mitra, U.; Eagar, T. Slag-metal Reactions during Welding: Part III. Verification of the Theory. *Metall. Trans. B* **1991**, *22*, 83–100. [CrossRef]
39. Coetsee, T. Phase Chemistry of Submerged Arc Welding (SAW) Fluoride Based Slags. *J. Mater. Res. Technol.* **2020**, *9*, 9766–9776. [CrossRef]
40. Glasser, F.; Osborn, E. Phase Equilibrium Studies in the System CaO-Cr_2O_3-SiO_2. *J. Am. Ceram. Soc.* **1958**, *41*, 358–367. [CrossRef]
41. Coetsee, T.; Mostert, R.J.; Pistorius, P.G.H.; Pistorius, P.C. The Effect of Flux Chemistry on Element Transfer in Submerged Arc Welding: Application of Thermochemical Modelling. *J. Mater. Res. Technol.* **2021**, *11*, 2021–2036. [CrossRef]
42. Zhang, J.; Wang, C.; Coetsee, T. Assessment of Weld Metal Compositional Prediction Models Geared Towards Submerged Arc Welding: Case Studies Involving CaF_2-SiO_2-MnO and CaO-SiO_2-MnO Fluxes. *Mater. Trans. B* **2021**, *52*, 2404–2415. [CrossRef]
43. Zhang, J.; Wang, C.; Coetsee, T. Thermodynamic Evaluation of Element Transfer Behaviors for Fused CaO-SiO_2-MnO Fluxes Subjected to High Heat Input Submerged Arc Welding. *Metall. Mater. Trans. B* **2021**, *52*, 1937–1944. [CrossRef]
44. Zhang, J.; Shao, G.; Guo, Y.; Xu, Q.; Liu,Z. Facilitating flux design process geared towards submerged arc welding via thermodynamic approach: Case study into CaF_2–SiO_2–Na_2O–Al_2O_3–TiO_2 agglomerated flux. *Calphad* **2022**, *79*, 102483.